Controlling Terahertz Emission from Quantum Wells†

Kevin L. Shuford and Jeffrey L. Krause*

University of Florida, Quantum Theory Project, P.O. Box 118435, Gainesville, Florida 32611-8435

Received: January 30, 2002

We show that quantum wells can be used as sources of controllable terahertz (THz) radiation. Excitation with an ultrafast laser pulse promotes charge carriers to the conduction band of a dc biased quantum well system. The induced wave packet oscillates back and forth through the structure and radiates in the THz frequency regime. In the devices considered, the radiation is tunable over a wide frequency range by varying the magnitude of the bias field. The amplitude of the emission can be altered by adjusting the frequency of the excitation laser. Pairs of phase-locked pulses can induce wave packets that interfere coherently with each other. The resulting THz signal is enhanced, diminished, or shifted by adjusting the delay time between excitation pulses. The THz emission can also be "sculpted" to possess desired characteristics. Two examples are considered in the text. First, we show that an optimized THz waveform can invert the population in a two-level system with a resonant π pulse. As a second example, we demonstrate selective population of vibrational levels in a diatomic molecule. Excitation to specific levels, as well as population of a desired distribution of levels, can be achieved. Finally, we discuss future applications of these ideas and the feasibility of using quantum well structures to produce intense, far-IR bursts of radiation.

1. Introduction

Considerable research over the past decade has been devoted to studies of carrier dynamics in semiconductors. One active area of research involves quantum-confined systems such as quantum wells, wires, and dots.[1] Experimental and theoretical investigations have surveyed topics such as resonant tunneling,[2,3] coherent oscillations,[4−8] Stark localization,[9,10] and terahertz (THz) emission.[11−13] These phenomena are of interest in both basic and applied research. They enable tests of fundamental concepts of quantum mechanics and offer the potential for technological applications and the design of novel devices. To be useful in device applications, the exotic effects observed to date must be observable and controllable. Several examples of quantum control in semiconductor devices have been reported recently, including control of photocurrents,[14,15] exciton density,[16,17] state population,[18−21] phonon emission,[22,23] and THz emission.[24−29] These are impressive examples of the ability to manipulate and actively control the quantum dynamics of charge carriers in the solid state.

Semiconductor nanostructures are of interest in the electronics industry due to their minute size and the availability of structures with customized properties for specific applications. Many examples are already in common use such as diodes, transistors, quantum well lasers, modulators, and switches. In this work, we consider the possibility that quantum wells can be used as sources (or detectors) of tunable, controllable THz radiation. Ultrafast pulses in this frequency regime are currently difficult to produce, and may find applications in spectroscopy, magnetic imaging, and optoelectronics.

When a quantum well structure is excited with a laser pulse of sufficient bandwidth, a coherent superposition state (or wave packet) of electronic levels is created in the conduction band. As the wave packet tunnels back and forth between wells, it emits radiation. For the devices considered here, the emission is typically in the THz regime. We show that this radiation can be controlled by varying the magnitude of the dc field and the parameters of the excitation pulse. Pairs of pulses can enhance or suppress the wave packet density and hence the magnitude of the THz radiation. This allows modifications of the frequency and amplitude of the emitted THz signal and optimization of the signal to achieve a specific goal. As examples, we show that properly tailored THz radiation can be used to invert the population in a two-level system and selectively excite vibrational states in a diatomic molecule.

2. Theory

In this section we review briefly the perturbative treatment of charge carrier dynamics in semiconductor heterostructures. This method agrees well with experiment and the more traditional density matrix description of transport in quantum wells.[30,31] Charge carriers are represented as wave packets that obey the time-dependent Schrödinger equation. Dynamics in two bands, coupled by a dipole operator, are described by the following set of equations

$$i\hbar|\dot{\Psi}_{\mathrm{h}}(t)\rangle = H_{\mathrm{h}}|\Psi_{\mathrm{h}}(t)\rangle - \mu\epsilon(t)|\Psi_{\mathrm{e}}(t)\rangle \tag{1}$$

and

$$i\hbar|\dot{\Psi}_{\mathrm{e}}(t)\rangle = H_{\mathrm{e}}|\Psi_{\mathrm{e}}(t)\rangle - \mu\epsilon(t)|\Psi_{\mathrm{h}}(t)\rangle \tag{2}$$

where $\epsilon(t)$ is the laser pulse, μ is the transition dipole moment, and $H_{\mathrm{h,e}}$ and $\Psi_{\mathrm{h,e}}$ are the Hamiltonians and wave functions for the heavy holes (labeled h) and the electrons (labeled e). These equations can be simplified by assuming that the laser intensity is in the perturbative (weak response) regime. In this case, the electronic population scales linearly with the pulse amplitude. As a result, the transition term in eq 1 is negligible with respect to the field-free Hamiltonian. Thus, the heavy hole wave function behaves essentially as an eigenstate, and its probability

† Part of the special issue "R. Stephen Berry Festschrift".

10.1021/jp020283c CCC: $22.00 © 2002 American Chemical Society
Published on Web 08/15/2002

density is stationary in time. Within this approximation, the equations are uncoupled, and the equation of motion for the electronic wave function can be approximated by using time-dependent perturbation theory.

In this work, we assume that the Coulomb interactions between the electrons and holes have a minimal effect on the dynamics and can be neglected. Previous studies of carrier dynamics have concluded that the Coulomb contribution to carrier dynamics in devices such as those considered here is small,[31] and that the intraband polarization leading to THz emission is influenced only slightly by excitonic effects.[32,33] In the absence of such effects, the electron dynamics can be treated exclusively in the confined dimension, *z*. The remaining degrees of freedom contribute only arbitrary, additive constants. The stationary states $|\phi_{j\alpha}\rangle$, for charge carriers confined within the quantum well structure satisfy a one-dimensional, effective-mass Schrödinger equation,[30,34]

$$\left\{\frac{-\hbar^2}{2m_\alpha^*}\frac{\partial^2}{\partial z^2} + V_\alpha(z) \pm eFz\right\}|\phi_{j\alpha}\rangle = E_{j\alpha}|\phi_{j\alpha}\rangle \tag{3}$$

where $\alpha = h$ or e, m_α^* is the effective mass, V_α is the confining potential, F is the magnitude of the static DC field, and $E_{j\alpha}$ is the energy. For electrons, the third term in the Hamiltonian has a negative sign, while for heavy holes, this term is positive. The effective masses are assumed to be $0.340m_e$ and $0.0665m_e$ for the heavy holes and electrons, respectively.[35,36] The wave packets can be expanded in stationary states as

$$|\Psi_\alpha(t)\rangle = \sum_j |\phi_{j\alpha}\rangle e^{-i\omega_{j\alpha}t} a_{j\alpha}(t) \tag{4}$$

where $\omega_{j\alpha} = E_{j\alpha}/\hbar$ and $a_{j\alpha}(t)$ are time-dependent coefficients. Inserting this expression into eq 2 gives the expansion coefficients as

$$\dot{a}_{ke}(t) = \frac{i\epsilon(t)}{\hbar}\sum_j a_{jh}(t)\langle\phi_{ke}|\mu|\phi_{jh}\rangle\, e^{i(\omega_{ke}-\omega_{jh})t} \tag{5}$$

Next we make the usual first-order approximation that the amount of population transferred is small. In this case, the coefficients in the summation remain close to their initial values. That is, $a_{1h} \approx 1$, and $a_{jh} \approx 0$ for $j \neq 1$. This gives the electronic wave packet coefficients as

$$a_{ke}(t) = \frac{i\mu_{k1}}{\hbar}\int_0^t dt'\, \epsilon(t')e^{i\omega_{k1}t'} \tag{6}$$

where $\mu_{k1} = \langle\phi_{ke}|\mu|\phi_{1h}\rangle$ and $\omega_{k1} = (\omega_{ke} - \omega_{1h})$. The functional form of the laser pulse is chosen as a Gaussian,

$$\epsilon(t) = E_0 e^{-(t-\bar{t})^2/2\Gamma^2}\cos[\omega(t-\bar{t})] \tag{7}$$

where E_0 is the pulse amplitude (arbitrary in perturbative limit), $\bar{t}$ is the center time, Γ is the pulse width, and ω is the carrier frequency. Inserting this expression into eq 6 and making the rotating wave approximation gives

$$a_{ke}(t) = \frac{i\mu_{k1}}{2\hbar}\int_0^t dt'\, E(t')e^{i\omega_{k1}t'} \tag{8}$$

where $E(t)$ is a complex laser pulse defined as

$$E(t) = E_0 e^{-(t-\bar{t})^2/2\Gamma^2} e^{-i\omega(t-\bar{t})} \tag{9}$$

The final expression for the electronic wave packet is then

$$|\Psi_e(t)\rangle = \frac{i}{2\hbar}\sum_k |\phi_{ke}\rangle\mu_{k1}\int_0^t dt'\, E(t')e^{-i\omega_{ke}(t-t')}e^{-i\omega_{1h}t'} \tag{10}$$

The electronic wave packet has a finite lifetime before dephasing (which is mainly due to carrier−carrier interactions) and destroys the coherence of the superposition state. Within the wave function formalism used here, true dephasing cannot be included. As an attempt to model the qualitative features of the observed physical behavior, the wave packet is multiplied by an exponential of the form

$$\psi = \Psi_e(t)e^{-\gamma(t-\bar{t})} \tag{11}$$

where $\gamma = 0.40\ \text{ps}^{-1}$. This value is consistent with intraband dephasing times calculated from numerical fits to data from GaAs/AlGaAs superlattices[33] and single quantum wells[37] under similar excitation conditions. The electronic wave packet begins decaying at the peak of the excitation pulse and has a lifetime of approximately 8 ps.

The oscillating wave packet creates an intraband polarization (time-dependent dipole moment) given by

$$d(t) = \langle\psi|ez|\psi\rangle \tag{12}$$

The coherent THz signal, E_{THz}, produced by this polarization is proportional to the second derivative of the dipole moment,

$$E_{THz} \propto \frac{\partial^2 d(t)}{\partial t^2} \tag{13}$$

The characteristics of this signal can be modified considerably, as demonstrated in the following sections.

3. Results

3.1. Tunable THz Emission. One way to control the THz emission from quantum wells is to use a fixed laser pulse and vary the dc field. The excitation pulse must have sufficient spectral bandwidth to coherently excite at least two electronic levels in the conduction band simultaneously. The two-state wave packet oscillates between the wells with a frequency $\Delta E/h$. The energy splitting of the two electronic levels, $\Delta E = E_2 - E_1$, governs the beat frequency and changes as a function of the magnitude of the static dc field. The range of frequencies that can be emitted is dictated by the dimensions of the structure, its material properties, and its response to the bias field.

As an example, we consider the asymmetric double quantum well (ADQW) in Figure 1. This structure has been the focus of numerous experimental and theoretical studies due to its simplicity, the availability of high-quality samples, and the abundance of data concerning its physical properties.[2,5,11,24,25,27,28] The model potential has a wide well of width 100 Å, a narrow well of width 80 Å, and a 20-Å barrier. The well depths and band gaps are based on parameters for GaAs and AlGaAs. Application of a dc bias field brings the two lowest energy levels in the conduction band into tunneling resonance. These levels undergo an avoided crossing as the field is increased from 0 to 40 kV/cm. In the valence band, the heavy hole levels diverge in energy as the field increases, which traps the holes in a single well. The properties of this system are well-known, making it a good candidate for preliminary studies regarding the possibilities of controlling THz emission in such a structure.

As a first example, the ADQW system is excited by a laser pulse with parameters $\bar{t} = 600$ fs, $\Gamma = 150$ fs, and a detuning

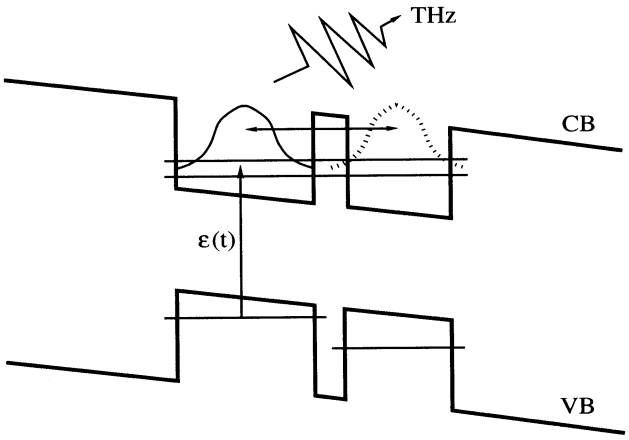

Figure 1. Schematic of the asymmetric double quantum well system considered in this work. Excitation occurs in the wide well from the valence band to the conduction band. The electronic wave packet oscillates through the narrow barrier between wells creating an intraband polarization, which is the source of the THz radiation.

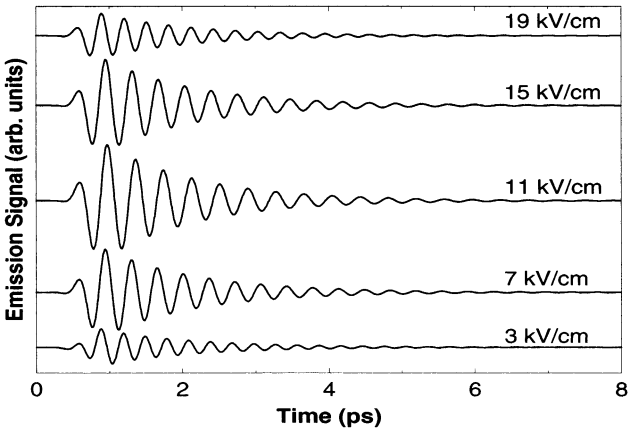

Figure 2. THz emission signals as a function of the magnitude of the static dc field. Identical excitation pulses were used for each signal, and the dc field was varied between 3 and 19 kV/cm. The tunneling resonance occurs at 11 kV/cm. At this value the signal is the most intense and shows the largest number of oscillations.

from the first electronic state of 1.32 THz. Note that the detuning is not the carrier frequency but is the difference between the carrier frequency and the energy of the first electronic state. With these pulse parameters, and for the dc fields considered here, a coherent superposition is created that is composed solely of the lowest two levels in the conduction band. These levels are dipole-coupled via the laser field to the highest energy heavy hole state in the valence band. Figure 2 shows the THz signals produced by the oscillating wave packet as a function of the magnitude of the dc field. As the dc field increases to 11 kV/cm, the splitting between the first two electronic levels decreases, which produces a longer oscillation period and deeper oscillations. At dc fields larger than 11 kV/cm, the energy splitting increases, which yields shorter periods and shallower oscillations. At 11 kV/cm the system is in tunneling resonance, with the smallest energy splitting and the deepest oscillations. The wells in the structure are strongly coupled at this point, with eigenstates very similar in character and energy, and completely delocalized across the structure. The excitation pulse coherently excites both stationary states with equal weight, and the most intense signal is observed. These results are qualitatively similar to experimental results observed previously.[11,13]

Further information about the effects of the dc field can be gleaned by examining the Fourier transforms of the traces in

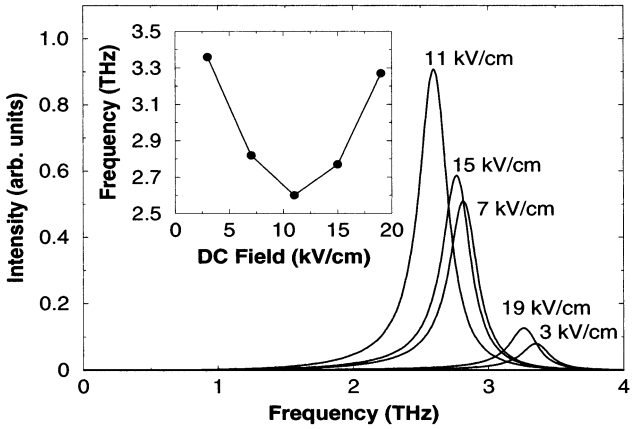

Figure 3. Fourier transforms of the emission signals in Figure 2. The inset shows the peak frequency present in the signals as a function of dc bias field. The spectrum at 11 kV/cm is at least 30% more intense than the other signals.

Figure 2. As seen in Figure 3, the peak observed with a bias field of 11 kV/cm is approximately 30% more intense than those produced at 7 and 15 kV/cm and approximately 6 times as intense as the remaining peaks. These figures indicate that at low and high values of the dc field, one eigenstate begins to dominate the coherent superposition, and the intensity of the signal decreases. Indeed, as seen in the figure the emission signals at 3 and 19 kV/cm are significantly weaker. In the limit that a single stationary state is excited, the THz emission vanishes.

As the results above indicate, the ADQW is a simple example of a tunable THz emitter or detector. The structure considered here has an emission range of ~2 THz, with varying signal intensities. Other semiconductor devices have also been shown to provide emission in this frequency regime. Several groups report the capability of various implementations of photoconducting antennas[38−40] and superlattices[13] to create bursts of THz radiation.

3.2. Signal Interference Effects. The properties of the coherent superposition state, or wave packet, that create the THz emission can be altered to vary the intensity of the emission. Excitation with a pair of phase-locked optical pulses offset by a delay time, τ, enables interferometric enhancement, annihilation, or phase shifting of the THz emission. The wave packets produced by each pulse are highly dependent on the relative phase of the excitation pulses. The magnitude of the THz signal is a function of the total wave packet density and will be enhanced or diminished by the interference between the excited waves. The intensity of two interacting waves with a time delay τ can be be written as

$$|A\cos(\omega t) + A\cos[\omega(t-\tau)]|^2 = A^2\cos^2(\omega t) + A^2\cos^2(\omega t - \omega\tau) + 2A^2\cos(\omega t)\cos(\omega t - \omega\tau) \quad (14)$$

$$= A^2\{\cos^2(\omega t) + [\cos(\omega t)\cos(\omega\tau) + \sin(\omega t)\sin(\omega\tau)]^2 + 2\cos(\omega t)[\cos(\omega t)\cos(\omega\tau) + \sin(\omega t)\sin(\omega\tau)]\} \quad (15)$$

For simplicity, we assume that both wave packets are produced by identical pulses. In this case, the amplitudes (A) and frequencies (ω) in the preceding equation are equal.

For the two-state wave packets considered previously in the ADQW, ω is the beat frequency, $\omega = (E_2 - E_1)/\hbar$. As can be seen in eq 15, the intensity of the wave depends sensitively on the delay time, τ. For the two waves to interfere constructively,

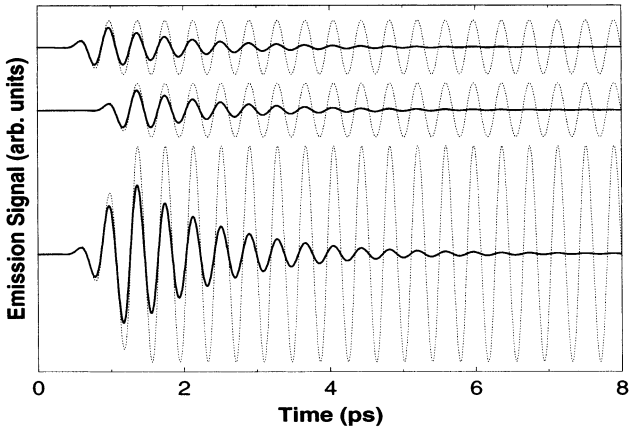

Figure 4. Coherent amplification of THz emission signals. The top two curves are the signals resulting from excitation with a single pulse. The bottom curve is the signal produced when both pulses are applied coherently with a phase difference of 2π. The signal is amplified by a factor of 4, indicating complete constructive interference. In each set of the signals, the solid lines include dephasing, while the dotted lines do not.

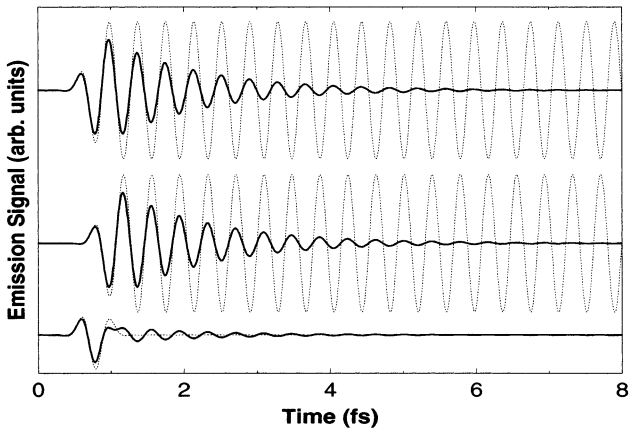

Figure 5. Coherent destruction of THz emission signals. The top two curves are the signals resulting from excitation with a single pulse. The bottom curve is the signal produced when both pulses are applied coherently with a phase difference of π. The signal is annihilated, indicating complete destructive interference. In each of the signals, the solid lines include dephasing, while the dotted lines do not.

the delay time between excitation pulses must equal the oscillation period (or a multiple of the period). For example, setting $\tau = 2\pi/\omega$ in eq 15 yields an intensity that is four times as intense as the signal from a single pulse. Destructive interference is also possible by adjusting the delay time to equal half of the oscillation period. Inserting $\tau = \pi/\omega$ into eq 15 produces complete annihilation of the THz signal. As shown in Figures 4 and 5, this simple analysis is adequate to describe the observed interference phenomena. In these figures, the relative phase between the wave packets has been adjusted to 2π and π, respectively, by varying the delay time. In both plots the solid lines include dephasing (with $\gamma = 0.40$ ps^{-1}), while the dotted lines ignore this effect ($\gamma = 0$). When dephasing is included, the decay of the signal obscures the full extent of the interference. However, the dotted lines clearly demonstrate the expected amplification by a factor of 4 for constructive interference and the complete cancellation of the signal for destructive interference. These results are in qualitative agreement with experiments demonstrating controlled THz emission.[24,25]

The simplified analysis does not describe the interference phenomena completely when the relative phase between the pulses is not an integer of π. When $\tau = 1.5\pi/\omega$, for example, the intensity expected from eq 15 is

$$A^2\{\cos^2(\omega t) + \sin^2(\omega t) - 2\cos(\omega t)\sin(\omega t)\} = A^2\{1 - \sin(2\omega t)\} \quad (16)$$

The intensity produced by a single pulse can be written as

$$A^2\cos^2(\omega t) = \frac{A^2}{2}[1 + \cos(2\omega t)] \quad (17)$$

indicating that THz signal with $\tau = 1.5\pi/\omega$ should be approximately twice as intense as that produced with a single pulse. However, as shown in Figure 6, the observed signal is approximately 3 times as intense as that for the single pulse. A pseudovector approach has been used previously to interpret signal intensities for cases of fractional π relative phases.[25,26] Note also in Figure 6 that the fractional phase difference induces a slight phase shift in the amplified signal compared to the first excitation pulse. In this example, the second pulse shifts the emission signal to about 50 fs earlier in time. This can be understood by writing eq 16 as

$$A^2\left[1 + \cos\left(2\omega t + \frac{\pi}{2}\right)\right] \quad (18)$$

which predicts a phase shift to earlier times by $\pi/2$. Our results display small phase shifts in all cases studied with fractional relative phases between the pulses. Under similar conditions, phase shifts as large as 330 fs have been observed experimentally.[24−26] Other experiments have demonstrated that pulse shaping and multiple pulses in series can amplify the THz signal significantly.[25−27] These results are intriguing illustrations of the use of pulse sequences with well-defined phase relations to amplify, destroy, or shift the THz emission from semiconductor heterostructures.

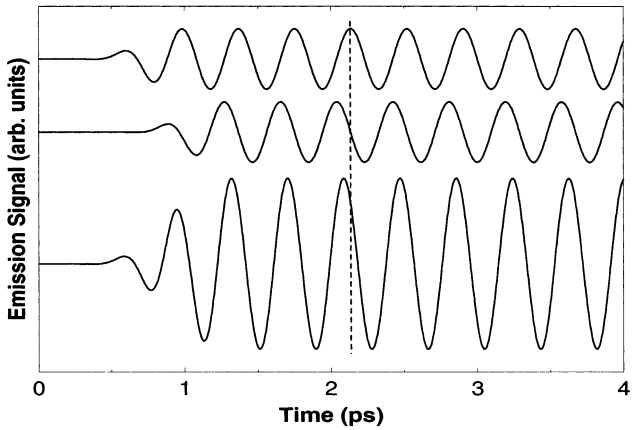

Figure 6. Coherent amplification of THz emission signals. The top two curves are the signals resulting from excitation with a single pulse. The bottom curve is the signal produced when both pulses are applied coherently with a phase difference of $3\pi/2$. The amplitude of the signal is enhanced by roughly a factor of 3. A phase shift of 50 fs compared to the top signal is also observed. Dephasing is neglected in this figure. The dashed line is included as an aid to visualization.

3.3. THz Applications. In this section we demonstrate that a carefully chosen excitation pulse can yield THz emission displaying desired characteristics. As demonstrated above, the frequency and amplitude of the signal can be tuned by adjusting the dc bias field and the center frequency of the excitation pulse. In principle, the phase and amplitude of the excitation pulse can be optimized as well.[41−43] The optimized field can then be

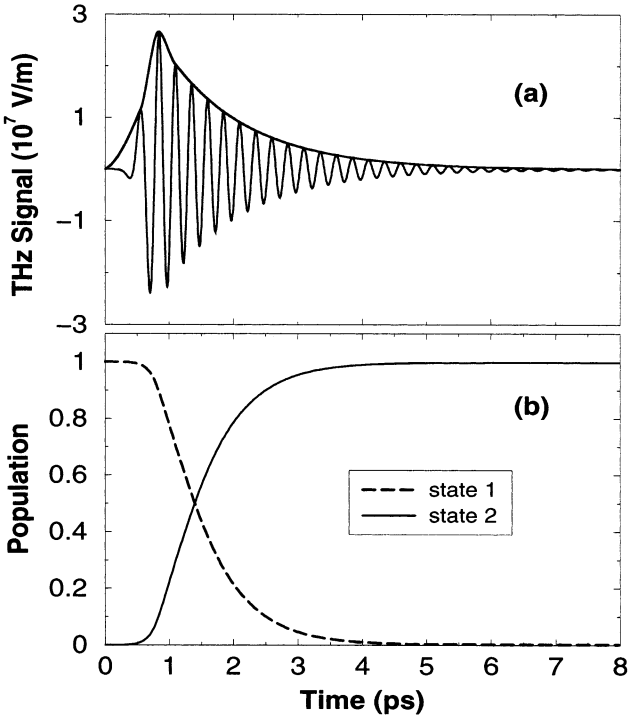

Figure 7. Sculpting of THz emission to invert population in a two-level system. The optimized THz radiation is shown in panel a, and the population dynamics in the two-level system are shown in panel b. The THz field has a pulse area of π, which completely inverts the population from the initial state to the final state.

applied to a system of interest and reoptimized if necessary to improve the performance in the actual physical system.[44]

As an example, we consider population control in a two-level system. The goal is to transfer population completely from one state to another using optimized THz emission as the excitation source. The two-level system is a generic case that might, for example, represent population transfer between rotational levels in molecules or Rydberg states in atoms. The solution to the problem of population inversion in two-level systems is well-known. With resonant excitation, complete population inversion is achieved if the area of the pulse is an odd multiple of π.[45,46] The inversion is robust with respect to the pulse shape, but not with respect to the area. The pulse area is defined as

$$\int_0^t \mathrm{d}t'\, \Omega_{21} = \int_0^t \mathrm{d}t' \frac{\langle 2|\mu|1\rangle}{\hbar} E(t') \tag{19}$$

where Ω_{21} is the Rabi frequency, $\langle 2|\mu|1\rangle$ is the transition dipole matrix element, and $E(t)$ is the laser pulse envelope.

We consider a two-level system with a resonant excitation frequency of 4 THz. To produce the required radiation, the ADQW in Figure 1 is biased with a dc field of 23.1 kV/cm. An optimized THz signal is produced by adjusting the center frequency of the excitation pulse to yield a THz pulse with area π. Figure 7 shows the optimized THz radiation and a population analysis of the test system. The excitation field induces complete population transfer from state $|1\rangle$ to $|2\rangle$, thus achieving the control objective. As expected, the unusual shape of the THz signal does not affect the efficiency of the population transfer. The population inversion is robust with respect to small changes in the pulse area. Some of the expected deviations caused, for example, by fluctuations in the polarization lifetime can be alleviated by adjusting the center frequency of the excitation laser.

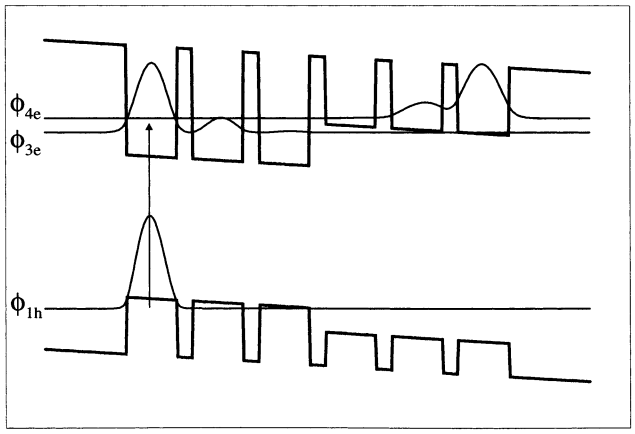

Figure 8. Schematic of a notched six-well structure with an applied bias field of 20 kV/cm. The heavy hole state as well as electronic states three and four are shown in the figure. This structure is designed to produce emission corresponding to the energies of several vibrational states of a light diatomic molecule.

Another possible application for THz pulses is spectroscopy in the linear regime. The population is not inverted completely, but significant control of the relative population of excited states is attainable. As an example, we consider vibrational state selectivity in a simple molecule. A Morse potential is used to model the potential energy for a diatomic molecule. The functional form of the Morse potential is

$$V(r) = D_e[1 - e^{-\beta(r-r_e)}]^2 \tag{20}$$

where D_e is the dissociation energy, r_e is the equilibrium bond distance, and β is a constant related to the vibrational frequency. In the example presented here, we choose $D_e = 500$ kJ/mol, $r_e = 2.75$ Å, and $\beta = 0.67$ Å^{-1}. With a reduced mass of 20 atomic mass units, the fundamental vibrational frequency is 250 cm^{-1}. The fourth overtone has a frequency of $4.95\omega_e$, demonstrating the characteristic effects of anharmonicity. The dipole moment operator is a function of distance and is assumed to be

$$\mu(r) = \mu_0 r e^{-ar^2} \tag{21}$$

where μ_0 and a are constants chosen to represent a given diatomic molecule. In this example, we choose $\mu_0 = e^{0.5}/r_e$ and $a = 1/(2r_e^2)$. This function rises rapidly from 0 at the origin to a maximum at the equilibrium bond distance and decreases slowly as the potential becomes more anharmonic. The parameters chosen for the potential and dipole moment are typical for light diatomic molecules. They can be varied easily to model a desired molecule for a specific application.

A modified quantum well structure was designed to produce the vibrational frequencies near the bottom of the molecular potential. Figure 8 shows a schematic of a notched, six-well structure. Each well is 65 Å wide and the barriers are 20 Å wide. The unusual shape of this structure produces eigenvalues with a nontrivial response to the dc field. In the absence of a dc field, states 1−3 and states 4−6 are close in energy, while a larger energy gap exists between states 3 and 4. The states begin to converge in energy as the dc field increases, with states 3 and 4 interacting first at ~35 kV/cm. As can be seen in the figure, exotic THz profiles can be created that contain a large range of frequencies. With an appropriate laser pulse, it is possible to excite only states 3 and 4, which yields a single-frequency signal. This signal can be tuned to match several vibrational states in the diatomic. Alternatively, signals contain-

TABLE 1: Parameters and Results for Relative Population Control of a Diatomic Molecule[a]

dc	ω	Γ	signal	P_1	P_2	P_3	P_4
28	18.6	95	250	0.98	0.02	10^{-5}	10^{-7}
20	18.4	85	498	10^{-6}	1.0	10^{-6}	10^{-9}
12	19.1	75	744	10^{-4}	0.067	0.93	10^{-6}
3	20.8	65	995	10^{-3}	0.47	0.014	0.52
28	29.7	35	214, 683	0.19	0.80	0.01	10^{-6}
20	19.7	35	163, 674, 841	0.78	0.13	0.09	10^{-6}
12	19.7	35	120, 879, 1007	0.06	0.85	0.09	10^{-4}
3	23.0	35	996, 1090, 1071, 1199	7.5×10^{-3}	0.66	9.4×10^{-3}	0.32

[a] The left side of the table shows the excitation parameters for the quantum well structure shown in Figure 8. The units for the dc field, frequency detuning, and pulse width are kV/cm, THz, and fs, respectively. The middle section shows the dominant frequencies present in the Fourier transform of the induced signal in units of cm^{-1}. The right side shows the relative populations of the vibrational states by the pulses in the diatomic molecule discussed in the text. The subscripts label the vibrational quantum numbers.

ing multiple frequencies can be produced to excite a distribution of vibrational levels.

The vibrational state distributions created by the THz signals are highly dependent on the dc field and the laser pulse that excites the quantum well. Table 1 shows the vibrational populations produced by excitation with various parameter sets. Using the correct combination of dc field and laser parameters yields THz signals resonant with the transition from the ground state to several vibrational levels in the diatomic. As can be seen in the table, essentially complete transfer of the excited population to $\nu = 1$, 2, or 3 is possible. The procedure is most successful at populating the $\nu = 2$ state due to the large dipole matrix element coupling this state to the ground state. The population of $\nu = 2$ as a function of time rises rapidly to 1, while other vibrational states are not populated significantly at any time. Populating levels $\nu = 1$ or 3 (with an appropriate parameter set) gives final time populations of 0.98 and 0.93, respectively. The intermediate time dynamics are considerably different than in the $\nu = 2$ example. In both cases, the population of $\nu = 2$ increases rapidly and begins to oscillate at early times. As the THz pulse ends, $\nu = 2$ decays, and the target state is populated. This impulsive excitation of $\nu = 2$ is found in all of the single-frequency studies.

As can be seen in Table 1, the lowest three excited vibrational states can be populated with high selectivity. However, due to the anharmonicity in the potential and the form and magnitude of the dipole moment, the same quantum well structure cannot be used to excite higher-lying states. Populating $\nu = 4$, for example, is not nearly as efficient or selective as $\nu = 1-3$. Creating a THz signal containing the resonant frequency does not induce the same selectivity as observed in the excitation of lower vibrational levels. This is due to several effects. For one, the THz signal overlaps more than one state as the energy levels become closer together. The dipole matrix element is also 2 orders of magnitude smaller than for the $\nu = 2$ state. As a result, the population is essentially shared between $\nu = 2$ and 4, as can be seen in the table. The impulsive excitation of $\nu = 2$ is dominant in this case, producing a superposition state that cannot be coerced into a single vibrational level. Energy levels greater than $\nu = 5$ cannot be populated with the current six-well structure. However, it is likely that, as in $\nu = 4$, the selectivity and efficiency will be reduced for these states due to the weak coupling to the initial state as ν increases.

Several trends are observed in the laser pulses used to excite the quantum well structure that produces the optimized THz signals. The frequencies and widths of the pulses are generally

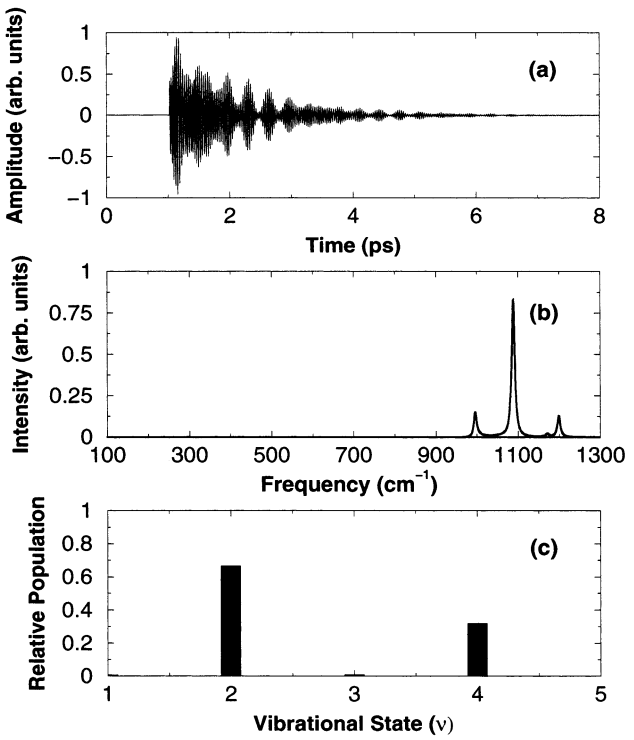

Figure 9. Emitted THz signal from the six-well structure in Figure 8 with a bias field of 3 kV/cm. Panel a shows the signal in the time domain, and panel b shows the Fourier transform to the frequency domain. Several frequencies are evident in the THz pulse. Panel c shows an analysis of the relative populations in the diatomic molecule produced by the pulse in panel a.

those that yield the most intense signal, with a single oscillation frequency. The clearest trend is the decrease of bandwidth (increased Γ) with increasing dc fields. In this example, the dc field causes the energy levels to move together. To excite just two electronic levels (1 frequency in signal) the bandwidth must decrease. A slight increase in laser frequency is also observed as the dc field decreases. It is difficult to interpret the frequency shifts, because the component eigenstates of the wave packet also vary as a function of the dc field.

Exciting the diatomic molecule with a THz signal composed of multiple frequencies produces population in several vibrational states. The lower portion of Table 1 contains population data from THz signals in which more than one frequency is present. With the dc field set to 28, 20, or 12 kV/cm, the population is distributed among three vibrational levels. Further, in each case the majority of population is in a state that was not significantly populated by single-frequency THz pulses at the same dc field. Figure 9 shows the THz signal from the final entry in Table 1. It is evident from the time and frequency domain representations that the signal is composed of several frequencies. This particular waveform produces a distribution of vibrational states in which the populations alternate in magnitude. The most intense frequencies in the pulse are in the region resonant with $\nu = 4$ or 5. However, at the end of the pulse, $\nu = 2$ has the largest population. This example demonstrates once again the importance of the dipole matrix element. Even with intense peaks resonant with higher lying vibrational levels, the population prefers to occupy a state strongly coupled to the ground state.

The notched six-well system is a versatile structure that can produce a wide variety of THz signals with numerous frequencies. This work shows that with a small number of parameters, the population of vibrational energy levels in a diatomic

molecule can be shifted from a single state to many states using optimized THz pulses. The final result depends sensitively on the qualities of the THz signal, which can be sculpted to obtain a desired control objective. Population inversion in a two-level system and state-selective excitation are two possible applications of THz radiation. The low power of existing sources has limited most applications to date to linear, time-domain spectroscopy, imaging, and communication.[47−49] However, in recent years several groups have reported the ability to shape and enhance narrow-band THz radiation.[48,50,51] Shaped THz pulses have been used to study resonant population transfer among Rydberg states in Cesium.[52] The increased power and short duration of new THz sources have enabled applications in nonlinear optics and multiphoton spectroscopy.[51] As further progress occurs in pulse enhancement and shaping, semiconductor structures may realize their potential as controllable sources of tunable electric fields in the far IR wavelength regime.

4. Conclusions

In this work we demonstrate that control of THz radiation emitted from quantum wells can be achieved by using simple, experimentally feasible laser pulses. The frequency of the emission is tunable over a large range by varying the magnitude of the static dc field. The amplitude of the emission can be altered by tuning the excitation frequency. Pairs of pulses can amplify or suppress the signal intensity. Phase-locked pulses with the proper delay times yield signals up to 4 times as intense as the signal produced with a single pulse. Alternatively, the signal can be completely annihilated. Phase shifts in the THz signal can be produced by setting the relative phase between the excitation pulses to a noninteger multiple of π. We also find that THz signals with desired characteristics can be produced by varying the excitation conditions. The emission signal can be optimized to achieve a predetermined goal in a system of interest, such as population transfer in a two-level system or state-selective excitation in a diatomic molecule. As examples, we showed that a carefully constructed THz field can invert the population in a two-level system and can actively control the relative population of several vibrational states in a model Morse oscillator.

Many other applications of sculpted THz radiation are feasible. This work is a first step toward analyzing what might be possible. Future work will consider additional examples of potential technological significance. We believe that such applications will become experimentally accessible as further advances are made in increasing the power of the sources and developing efficient means to shape THz pulses.

Acknowledgment. We are pleased to dedicate this paper to Prof. R. Stephen Berry on the occasion of his 70th birthday. One of us (J.L.K.) values greatly the time he spent as a graduate student in Steve's group. Steve's deep physical insight, wide-ranging interests, and good humor are an inspiration to us all. We acknowledge useful comments and suggestions from David Reitze. This work was partly supported by the National Science Foundation through Grant CHE-9875080. J.L.K. is a Cottrell Scholar of the Research Corporation.

References and Notes

(1) Shah, J. *Ultrafast Spectroscopy of Semiconductors and Semiconductor Nanostructures*; Springer: New York, 1999.

(2) Heberle, A. P.; Rühle, W. W.; Köhler, K. *Phys. Status Solidi B* **1992**, *173*, 381.

(3) Heberle, A. P.; Rühle, W. W.; Alexander, M. G. W.; Köhler, K. *Semicond. Sci. Technol.* **1992**, *7*, B421.

(4) Leo, K.; Damen, T. C.; Shah, J.; Göbel, E. O.; Köhler, K. *Appl. Phys. Lett.* **1990**, *57*, 19.

(5) Leo, K.; Shah, J.; Göbel, E. O.; Damen, T. C.; Schmitt-Rink, S.; Schäfer, W.; Köhler, K. *Phys. Rev. Lett.* **1991**, *66*, 201.

(6) Dignam, M.; Sipe, J. E.; Shah, J. *Phys. Rev. B* **1994**, *49*, 10502.

(7) Dekorsy, T.; Leisching, P.; Köhler, K.; Kurz, H. *Phys. Rev. B* **1994**, *50*, 8106.

(8) Leisching, P.; Bolivar, P. H.; Beck, W.; Dhaibi, Y.; Brüggermann, F.; Schwedler, R.; Kurz, H.; Leo, K.; Köhler, K. *Phys. Rev. B.* **1994**, *50*, 14 389.

(9) Mendez, E. E.; Agulló-Rueda, F.; Hong, J. M. *Phys. Rev. Lett.* **1988**, *60*, 2426.

(10) Dignam, M. M.; Sipe, J. E. *Phys. Rev. B* **1991**, *43*, 4097.

(11) Roskos, H. G.; Nuss, M. C.; Shah, J.; Leo, K.; Miller, D. A. B.; Fox, A. M.; Schmitt-Rink, S.; Köhler, K. *Phys. Rev. Lett.* **1992**, *68*, 2216.

(12) Planken, P. C. M.; Nuss, M. C.; Brener, I.; Goossen, K. W.; Luo, M. S. C.; Chuang, S. L.; Pfeiffer, L. *Phys. Rev. Lett.* **1992**, *69*, 3800.

(13) Waschke, C.; Roskos, H. G.; Schwedler, R.; Leo, K.; Kurz, H.; Köhler, K. *Phys. Rev. Lett.* **1993**, *70*, 3319.

(14) Kurizki, G.; Shapiro, M.; Brumer, P. *Phys. Rev. B* **1989**, *39*, 3435.

(15) Dupont, E.; Corkum, P. B.; Liu, H. C.; Buchanan, M.; Wasilewski, Z. R. *Phys. Rev. Lett.* **1995**, *74*, 3596.

(16) Heberle, A. P.; Baumberg, J. J.; Köhler, K. *Phys. Rev. Lett.* **1995**, *75*, 2598.

(17) Cundiff, S. T.; Knorr, A.; Feldmann, J.; Koch, S. W.; Göbel, E. O.; Nickel, H. *Phys. Status Solidi B* **1995**, *188*, 307.

(18) Pötz, W. *Appl. Phys. Lett.* **1997**, *71*, 395.

(19) Dargys, A. *Phys. Status Solidi B* **2000**, *219*, 401.

(20) Binder, R.; Lindberg, M. *Phys. Rev. Lett.* **1998**, *81*, 1477.

(21) Hohenester, U.; Troiani, F.; Molinari, E.; Panzarini, G.; Macchiavello, C. *Appl. Phys. Lett.* **2000**, *77*, 1864.

(22) Hu, X.; Pötz, W. *Phys. Rev. Lett.* **1999**, *82*, 3116.

(23) Wehner, M. U.; Ulm, M. H.; Chemla, D. S.; Wegener, M. *Phys. Rev. Lett.* **1998**, *80*, 1992.

(24) Planken, P. C. M.; Brener, I.; Nuss, M. C.; Luo, M. S. C.; Chuang, S. L. *Phys. Rev. B.* **1993**, *48*, 4903.

(25) Luo, M. S. C.; Chuang, S. L.; Planken, P. C. M.; Brener, I.; Nuss, M. C. *Phys. Rev. B.* **1993**, *48*, 11043.

(26) Brener, I.; Planken, P. C. M.; Nuss, M. C.; Luo, M. S. C.; Chuang, S. L.; Pfeiffer, L.; Leaird, D. E.; Weiner, A. M. *J. Opt. Soc. Am. B* **1994**, *11*, 2457.

(27) Weiner, A. M. *J. Opt. Soc. Am. B* **1994**, *11*, 2480.

(28) Pötz, W. *App. Phys. Lett.* **1998**, *72*, 3002.

(29) Tamborenea, P. I.; Metiu, H. *J. Chem. Phys.* **1999**, *110*, 9202.

(30) Krause, J. L.; Reitze, D. H.; Sanders, G. D.; Kuznetsov, A. V.; Stanton, C. J. *Phys. Rev. B* **1998,** *57*, 9024.

(31) Shuford, K. L.; Krause, J. L. *J. Appl. Phys.* **2002**, *91*, 6533.

(32) Meier, T.; von Plessen, G.; Thomas, P.; Koch, S. W. *Phys. Rev. Lett.* **1994**, *73*, 902.

(33) Leisching, P.; Dekorsy, T.; Bakker, H. J.; Kurz, H. *Phys. Rev. B* **1995**, *51*, 18 015.

(34) Kuznetsov, A. V.; Sanders, G. D.; Stanton, C. J. *Phys. Rev. B* **1995**, *52*, 12 045.

(35) Miller, D. A. B.; Chemla, D. S.; Damen, T. C.; Gossard, A. C.; Wiegmann, W.; Wood, T. H.; Burrus, C. A. *Phys. Rev. B* **1985,** *32*, 1043.

(36) Fox, A. M.; Miller, D. A. B.; Livescu, G.; Cunningham, J. E.; Henry, J. E.; Jan, W. Y. *Phys. Rev. B.* **1990**, *42*, 1841.

(37) Schultheis, L.; Honold, A.; Kuhl, J.; Köhler, K.; Tu, C. W. *Phys. Rev. B* **1986**, *34*, 9027.

(38) Fattinger, C.; Grischkowlky, D. *Appl. Phys. Lett.* **1988**, *53*, 1480.

(39) Auston, D. H.; Cheung, K. P.; Smith, P. R. *Appl. Phys. Lett.* **1984**, *45*, 284.

(40) Hu, B. B.; Darrow, J. T.; Zhang, X. C.; Auston, D. H. *Appl. Phys. Lett.* **1990**, *56*, 886.

(41) Weiner, A. M.; Heritage, J. P.; Kirschner, E. M. *J. Opt. Soc. Am. B* **1988**, *5*, 1563.

(42) Hillegas, C. W.; Tull, J. X.; Goswami, D.; Strickland, D.; Warren, W. *Opt. Lett.* **1994**, *19*, 737.

(43) Wefers, M. M.; Nelson, K. A. *Opt. Lett.* **1993**, *18*, 2032.

(44) Judson, R. S.; Rabitz, H. *Phys. Rev. Lett.* **1992**, *68*, 1500.

(45) Allen, L.; Eberly, J. H. *Optical Resonance and Two-Level Atoms*; John Wiley & Sons: New York, 1975.

(46) Milonni, P. W.; Eberly, J. H. *Lasers*; John Wiley & Sons: New York, 1988.

(47) Heyman, J. N.; Kersting, R.; Unterrainer, K. *Appl. Phys. Lett.* **1998**, *72*, 644.

(48) Liu, Y.; Park, S.; Weiner, A. M. *Opt. Lett.* **1996**, *21*, 1762.

(49) Weling, A. S.; Hu, B. B.; Froberg, N. M.; Auston, D. H. *Appl. Phys. Lett.* **1994**, *64*, 137.

(50) van Exter, V.; Fattinger, C.; Grischkowsky, D. *Appl. Phys. Lett.* **1989**, *55*, 337.

(51) You, D.; Jones, R. R.; Dykaar, D.; Bucksbaum, P. *Opt. Lett.* **1993**, *18*, 290.

(52) Raman, C.; DeCamp, M. F.; Bucksbaum, P. H. *Opt. Express* **1997**, *1*, 186.